ISSN: (Print) (Online) Journal homepage: <https://www.tandfonline.com/loi/tbsd20>

Effects of glycans and hinge on dynamics in the IgG1 Fc

Christina Bergonzo, J. Todd Hoopes, Zvi Kelman & D. Travis Gallagher

To cite this article: Christina Bergonzo, J. Todd Hoopes, Zvi Kelman & D. Travis Gallagher (28 Oct 2023): Effects of glycans and hinge on dynamics in the IgG1 Fc, Journal of Biomolecular Structure and Dynamics, DOI: [10.1080/07391102.2023.2270749](https://doi.org/10.1080/07391102.2023.2270749)

To link to this article: <https://doi.org/10.1080/07391102.2023.2270749>



View supplementary material [↗](#)



Published online: 28 Oct 2023.



Submit your article to this journal [↗](#)



View related articles [↗](#)



View Crossmark data [↗](#)



Effects of glycans and hinge on dynamics in the IgG1 Fc

Christina Bergonzo^a, J. Todd Hoopes^b, Zvi Kelman^{a,b} and D. Travis Gallagher^a

^aInstitute for Bioscience and Biotechnology Research, National Institute of Standards and Technology, The University of Maryland, Gudelsky Way, Rockville, MD, USA; ^bBiomolecular Labeling Laboratory, Institute for Bioscience and Biotechnology Research, National Institute of Standards and Technology, The University of Maryland, Gudelsky Way, Rockville, MD, USA

Communicated by Ramaswamy H. Sarma

ABSTRACT

The crystallizable fragment (Fc) domain of immunoglobulin subclass IgG1 antibodies is engineered for a wide variety of pharmaceutical applications. Two important structural variables in Fc constructs are the hinge region connecting the Fc to the antigen binding fragments (Fab) and the glycans present in various glycoforms. These components affect receptor binding interactions that mediate immune activation. To design new antibody drugs, a robust *in silico* method for linking stability to structural changes is necessary. In this work, all-atom simulations were used to compare the dynamic behavior of the four structural variants arising from presence or absence of the hinge and glycans. We expressed the simplest of these constructs, the 'minimal Fc' with no hinge and no glycans, in *Escherichia coli* and report its crystal structure. The 'maximal Fc' that includes full hinge and G0F/G1F glycans is based on a previously reported structure, Protein Data Bank (PDB) ID: 5VGP. These, along with two intermediate structures (with only the glycans or with only the hinge) were used to independently measure the stability effects of the two structural variables using umbrella sampling simulations. Principal component analysis (PCA) was used to determine free energy effects along the Fc's dominant mode of motion. This work provides a comprehensive picture of the effects of hinge and glycans on Fc dynamics and stability.

ARTICLE HISTORY

Received 11 July 2023
Accepted 8 October 2023

KEYWORDS

Molecular dynamics; crystallography; monoclonal antibody; glycosylation; free energy of interaction; protein structure

Introduction

Immunoglobulins of subclass IgG1 make up the majority of therapeutic monoclonal antibody (mAb) drugs. The IgG1 protein is a 150 kDa tetramer, consisting of two heavy chains (HC) and two light chains (LC) covalently linked by disulfide bonds (Figure 1). Each antigen binding region (Fab) consists of a whole LC and half of an HC. The remaining halves of the two HC form the Fc, which induces immune system activation by binding to various receptors. The flexible linker between the Fabs and the Fc is the hinge; its two disulfide bonds are the only covalent connection between the HC. To enable biopharmaceutical companies to perform the types of analysis required during product development and for FDA approval, NIST Reference Material (RM) 8671, called the NISTmAb, was developed from an IgG1 κ mAb (Schiel et al., 2014, 2018). The structure of the NISTmAb Fc homodimer has been reported and is in the Protein Data Bank (rcsb.org) as 5VGP, along with about 100 other human Fc structures (Gallagher et al., 2018). In 5VGP as in nearly all Fc crystal structures, the hinge is present but unobserved due to its mobility. In an Fc, each chain forms two domains, CH2 and CH3, connected by an outward-projecting loop called the elbow. The two chains interact noncovalently through an extensive interface between the C-terminal CH3 domains.

The two halves also interact through their asparagine-linked (N-linked) glycans attached at Asn300 in the CH2 domain, and in the hinge (Figure 1). The dimer is flexible within each chain at the elbow, giving the CH2 domains freedom to swing independently with respect to the CH3 dimer. This intrinsic flexibility is confirmed through analysis of Fc structure coordinates deposited in the Protein Data Bank (rcsb.org), where the distance between the CH2 domain centers of mass ranges from 32 Å to 39 Å (Supplementary Figure 1 and Supplementary Table 1). The CH2-CH3 interface has been described as a ball-and-socket joint (Chiu et al., 2019), and while long timescale molecular dynamics (MD) simulations have been performed on Fc domains, the results state that the motion of Fc remains undersampled due to the complexity of this large dimeric glycoprotein (Frank et al., 2014).

Two key targets of engineered IgG proteins in general and the Fc domain in particular are glycans and disulfides. The N-linked glycans have been reported to affect Fc dynamics (Russell et al., 2018), and glycoengineering of therapeutic antibodies has become an active area of therapeutic research (Kiyoshi et al., 2017). The hinge region of IgG1 Fc is important to the full molecule's conformational dynamics and is in part characterized by two inter-strand disulfide crosslinks in the core 'CPPCP' motif. In crystal structures of the isolated Fc

CONTACT Christina Bergonzo  christina.bergonzo@nist.gov

 Supplemental data for this article can be accessed online at <https://doi.org/10.1080/07391102.2023.2270749>.

The work of Christina Bergonzo, Zvi Kelman and D. Travis Gallagher was authored as part of his official duties as an Employee of the United States Government and is therefore a work of the United States Government. In accordance with 17 USC. 105, no copyright protection is available for such works under US Law. J. Todd Hoopes hereby waive their right to assert copyright, but not their right to be named as coauthors in the article.

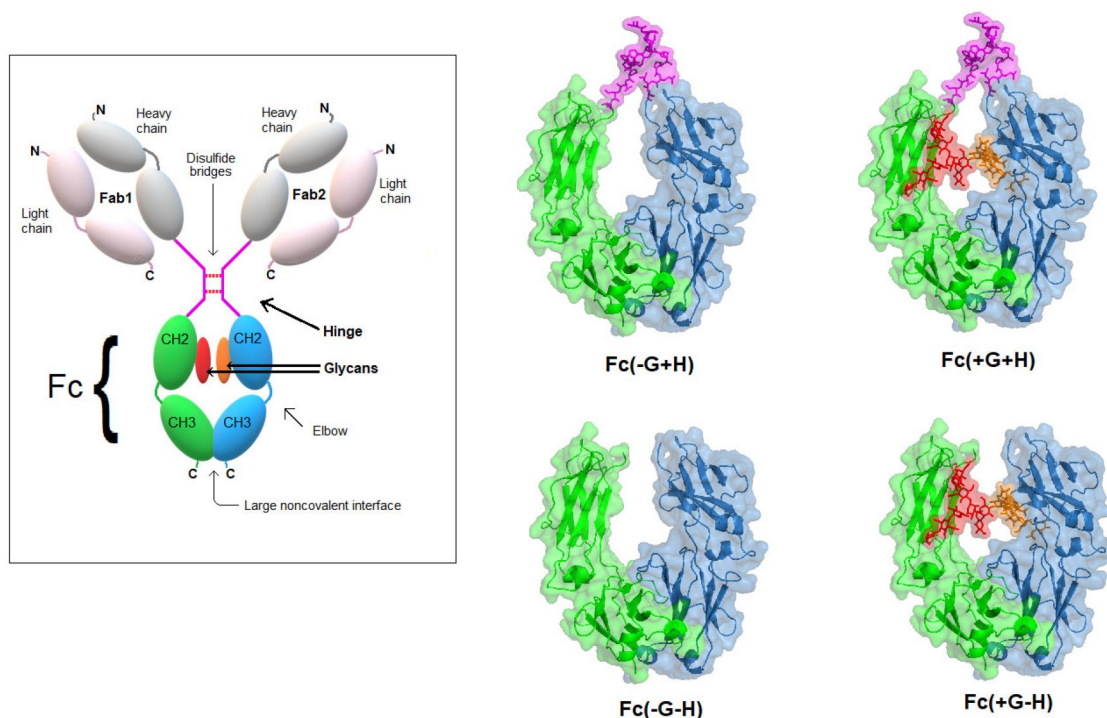


Figure 1. Inset panel: Diagram showing key parts of an IgG1 antibody. N and C termini of each chain are labeled. The Fc domain comprises the CH2 and CH3 domains of both heavy chains. Glycans (red and orange ovals) are attached to the CH2 domains. The hinge (magenta) contains two disulfide bridges that are the only covalent connections between the heavy chains. (The antibody has 14 additional disulfide bridges that are not shown.) The four Fc forms studied in this work, featuring the presence or absence of glycans (colored red and orange) and hinge (colored magenta). Sources of initial coordinates are described in the Methods section.

domain the hinge is largely unstructured and missing density, even though it is generally present in those crystals. As a result, the hinge conformational properties and its contribution to Fc domain dynamics remain largely unknown and structurally under-characterized, though it remains a target for engineering (Dall'Acqua et al., 2006; Presta, 2008; Yan et al., 2012). Both glycans and the disulfide containing hinge have been targets of mutagenesis attempting to exert therapeutic control over the human immune response (Deveuve et al., 2020; Valeich et al., 2020). Additionally, current 'Fc-fusion' drugs on the market, including Enbrel® (etanercept), retain the antibody hinge region and Fc domain while attaching a polypeptide drug product, in order to prevent degradation and extend the serum half-life of the drug (Duivelshof et al., 2021; Jafari et al., 2017). We can also consider functionalized Fc domains, which have been independently optimized to contain antigen binding sites while retaining the biophysical properties of the Fc, including effector functions and increased half-life (Traxlmayr et al., 2011; Wozniak-Knopp et al., 2010). In general, the functional accessibility of the drug moieties depends on the geometry and dynamics of the hinge and Fc.

Molecular dynamics (MD) studies have been performed to characterize the Fc domain (Frank et al., 2014; Lai et al., 2014; Lee & Im, 2017; Ma, 2021; Yanaka et al., 2019). State-of-the-art force fields and explicit solvent, and in some cases enhanced sampling with replica exchange MD (Harbison & Fadda, 2020) were used to characterize the conformational variability between each chain's CH2 and CH3 domains and to map the carbohydrate conformations and contacts (Buck

et al., 2013; Frank et al., 2014; Kiyoshi et al., 2015; Losonczi & Prestegard, 1998). Each of these studies, though limited to the local energy minimum described by various crystal structures of Fc, yield significant insights into the ground state behavior of this important IgG1 domain. MD simulations were also used to generate conformational ensembles of the Fc domain that were validated through comparison to experimental SAXS profiles (Yanaka et al., 2019). This data showed that a single structure fit to experimental SAXS curves was inadequate to describe the conformational dynamics of Fc, and a multiconformational fit was necessary (Yanaka et al., 2019). To build on the above studies, stability measurements in terms of free energies are necessary to quantify stability, which has been primarily assessed until now through root mean square deviation (RMSD) and root mean square fluctuation (RMSF) measurements.

In this study, we use umbrella sampling molecular dynamics simulations to probe the stability of the Fc dimer and describe the contributions of various Fc constructs (detailed in Figure 1) using free energies. To enhance our knowledge of structural data for Fc constructs, we report the crystal structure of the NISTmAb human IgG1 Fc construct (at 2.0 Å resolution), expressed in *Escherichia coli*, absent glycans and the hinge. We find that while the hinge and glycans both stabilize the Fc overall, the hinge and glycans have distinct local effects that disrupt closed and open dimer conformations, respectively. We report the differences in Fc domain average conformational characteristics as well as free energies of opening for +/- hinge and +/- glycans, providing a robust picture of Fc domain dynamics under a range of

conditions. This technique can be used for reporting stability of the Fc domain due to changes in the protein, enabling fast analysis of subsequent proposed changes for engineering Fc domains.

Methods

Production of Fc(-G-H) in *E. coli*

A gene encoding the Fc fragment was designed to express the IgG1 heavy chain residues 238 to 450, with the first two residues replaced by Met-Ala. The gene was synthesized and cloned into a pET-21a vector by GeneArt (Thermo Fisher Scientific) to enable *E. coli* expression. The Fc gene was cloned between the NdeI and XhoI restriction sites with two stop codons upstream of the XhoI site, thus not including a tag in the expressed Fc. The Fc protein was expressed in Shuffle[®] Express cells (New England Biolabs) by incubating a single colony containing the plasmid overnight at 30 °C degrees with orbital shaking at 250 RPM. Two 4L baffled flasks containing Luria broth (LB) pre-warmed to 30 °C were inoculated with 20 mL of the overnight culture and shaken at 190 RPM until OD₆₀₀ 0.8. The cultures were then cooled on ice to 15 °C and allowed to grow (\approx 1 h) until an OD₆₀₀ 1.2 was reached. Expression was then induced by adding Isopropyl β -D-1-thiogalactopyranoside (IPTG) at 0.66 mmol/L final concentration. Cultures were allowed to express for approximately 35 h at 15 °C with shaking at 190 RPM, and then harvested by centrifugation at 5 000 \times *g* to yield approximately 19 g of wet cell paste that was recovered and stored at -80 °C.

To purify the protein the cells were lysed in three-fold concentrated (3 \times) phosphate-buffered saline (PBS) (5 mL/g wet cell mass) by two passes through a cell disruptor (Constant Systems Ltd.), operating at 172 mPa (25 000 psi). After disruption, phenylmethyl sulfonyl fluoride (PMSF) was added to 1 mmol/L, and the sample was centrifuged at 30 000 \times *g* for 30 min. Temperature was maintained below 10 °C during centrifugation. The supernatant was loaded onto a 5 mL Protein A column (MabSelect SureTM) equilibrated in 2 \times PBS. The column was washed with 5 column volumes (CV) of 2 \times PBS, 20% ethylene glycol, then eluted with 0.1 mmol/L sodium citrate, pH 3.1, and the eluent was pH-neutralized with 1 mol/L Tris pH 9.0 (100 μ L per mL of eluent). The protein was further purified by size exclusion chromatography using a Superdex-100 column equilibrated in 2 \times PBS and operating at 2.5 mL/min for 1.5 CVs. The peak at \approx 45 kDa was collected and contained the dimeric ecFc protein. The buffer of the protein sample was changed to 25 mmol/L histidine buffer using a desalting column. Prior to crystallization, the protein was dialyzed into 100 mmol/L NaCl, 25 mg/mL histidine, pH 6 for crystal screening.

Crystallization and structure determination

Crystal screening against about 300 conditions yielded clusters of rectangular bars from several polyethylene-glycol-plus-salt conditions near neutral pH. Optimization led to 20%

polyethylene glycol 6000, 40 mmol/L calcium chloride, 100 mmol/L Na \bullet HEPES, pH 7.0. Single crystals were harvested and cryocooled by plunging into liquid nitrogen and kept at 100 K through data collection at beamline 23-ID-D of the Advanced Photon Source at Argonne National Laboratory, where a diffraction dataset to 2.0 Å resolution was collected (see Table 1).

The structure was solved by molecular replacement using the program Phaser (McCoy et al., 2007), using an Fc starting model based on PDB entry 5VGP (Gallagher et al., 2018). The starting model was prepared by removing its termini and loops. These parts were then rebuilt to difference electron density maps in an iterative process, utilizing the crystallographic refinement suite CCP4.(Winn et al., 2011) The 14,000-nonhydrogen-atom structure underwent 10 rounds of refinement, each round comprising map inspection, model adjustments, cycles of global minimization using REFMAC (Murshudov et al., 1997), and calculation of a new map. Model adjustments gradually gave the model its own structure, fitting its own diffraction data and diverging from the 5VGP PDB entry coordinates by a heavy atom RMSD of 1.67 Å (Supplementary Figure 2) (Gallagher et al., 2018). The programs PYMOL (Schrödinger & DeLano, 2020) and VMD (Humphrey et al., 1996) were used for molecular graphics, model adjustments, and making Figures. Analysis of crystal contacts utilized PISA (Krissinel & Henrick, 2007). Refinement of the structure (Table 1) led to the final deposited model PDB:7RHO.

Molecular modeling and dynamics of Fc truncation mutants

Coordinates for the four systems studied using molecular dynamics were built from three different starting coordinate sets, the details of which are summarized in Figure 1 and

Table 1. Diffraction and refinement statistics for structure 7RHO.

PDB accession code	7rho
Data collection	
Space group	P 21 21 21
Unit cell lengths (Å)	52.84, 150.39, 241.43
Resolution range (Å) ^a	15.0 – 2.0 (2.12 – 2.0)
Total reflections	114,393 (10,100)
Multiplicity	11.0 (9.9)
R_{merge}^b	0.080 (1.639)
Mean $I/\sigma(I)$	15.3 (1.4)
Refinement	
Resolution range (Å)	15.0 – 2.0 (2.05 – 2.0)
Reflections used ^a	110,540 (4022)
R_{work}^c	0.220 (0.377)
R_{free}^c	0.270 (0.388)
Protein residues	1652
Protein atoms	13,162
Water molecules	665
r.m.s.d. from ideality:	
Bond lengths (Å)	0.007
Bond angles (°)	1.328
Ramachandran outliers	0
Clashscore	6.0
Average B factor (Å ²)	54.0

^aValues in parentheses correspond to the highest resolution shell.

^b $R_{\text{merge}} = \sum |I_i - \langle I \rangle| / \sum I_i$, where I_i is the intensity of an individual reflection and $\langle I \rangle$ is the average intensity of that reflection.

^c $R_{\text{work}}(R_{\text{free}}) = \sum ||F_o| - |F_c|| / \sum |F_o|$; 5.0% of data were used for R_{free} .

Table 2. Source of starting structures and their modifications for simulations in this work.

Structure	Origin of coordinates	Hinge	Glycans
Fc(+G + H)	NISTmAb model PDB	Yes	Yes
Fc(-G + H)	NISTmAb model PDB	Yes	No
Fc(+G-H)	5VGP PDB	No	Yes
Fc(-G-H)	7RHO (this work)	No	No

Table 2. Fc(+G + H) coordinates were built from NISTmAb PDB coordinates truncated to residue Thr228 on each heavy chain and include the CPPCP motif hinge region modeled from another mAb (PDB ID 1IGT (Harris et al., 1997)) and described in detail elsewhere (Bergonzo & Gallagher, 2021). Fc(-G + H) starting coordinates were identical to the Fc(+G + H) system, with the glycans on each Fc(+G + H) chain deleted. Fc(+G-H) coordinates were built from PDB entry 5VGP (Karageorgos et al., 2017). The Fc(-G-H) coordinates were built from the 7RHO PDB entry coordinates described above. For structures containing glycans, the glycans were G0F and G1F biantennary complex type glycans, attached on chains A and B, respectively, and were built based on the reported density in PDB ID 5VGP (Gallagher et al., 2018). The glycoforms used were consistent with quantified glycan distributions for the NISTmAb (Prien et al., 2015). Each set of starting coordinates (Fc(+G + H), Fc(-G + H), Fc(+G-H), and Fc(-G-H)) were pre-processed using PrepareforLeap (Roe & Bergonzo, 2022) to generate LEaP input files with disulfide and glycan bonding instructions. Coordinate files were built using LEaP with the ff19SB protein force field (Tian et al., 2020), the glycam 06j-1 carbohydrate force field (Kirschner et al., 2008), and solvated in an octahedral box with optimal point charge (OPC) waters using a 10 Å buffer from the solute to the edge of the solvent box (13383, 22145, 22328, and 15658 water molecules were added for the Fc(-G-H), Fc(+G,H), Fc(-G + H), and Fc(+G-H) systems, respectively) (Anandakrishnan et al., 2013). The Fc(+G-H) system was neutralized with two Cl⁻ ions, while the Fc(-G-H), Fc(-G + H), and Fc(+G + H) systems were neutral. An additional 75 Na⁺ ions and 75 Cl⁻ ions were added to each system to approximate a 150 mmol/L to 200 mmol/L NaCl solution (Sengupta et al., 2021). Ions were randomized 6.0 Å away from solute and 4.0 Å away from each other four times and their positions saved to a new coordinate file, with each coordinate file used to initiate a simulation. Four independent runs for each structure were minimized and solvent equilibrated using a combination of minimization and MD with decreasing positional restraints on the solute, in both NVT (canonical ensemble, constant number of molecules, constant volume, constant temperature) and NPT (isobaric-isothermal ensemble, constant number of molecules, constant pressure, constant temperature) ensembles, as specified in AmberEQUIL (Roe & Brooks, 2020).

Simulations of the intact NISTmAb were started from the model NISTmAb coordinates (Bergonzo & Gallagher, 2021). The ff14SB protein force field (Maier et al., 2015), glycam 06j-1 carbohydrate force field (Kirschner et al., 2008), and solvated in a cubic box with SPC/E waters to minimize the number of points in the system (vs. OPC) (Berendsen et al., 1987), using a 10 Å buffer from the solute to the edge of the

solvent box (102 215 water molecules added). The NISTmAb system was neutralized with 10 Cl⁻ ions, and an additional 367 Na⁺ and 367 Cl⁻ ions were added to approximate a 150 mmol/L solution (Joung & Cheatham, 2008). Ions were randomized 6.0 Å away from solute and 4.0 Å away from each other four times, with each restart used to initiate a simulation. Four independent runs for each structure were minimized and solvent equilibrated using a combination of minimization and MD with decreasing positional restraints on the solute, in both NVT and NPT ensembles, as specified in AmberEQUIL (Roe & Brooks, 2020).

MD simulations in the NVT ensemble were run for 1 μs using Amber20 pmemd.cuda.MPI (Salomon-Ferrer et al., 2013), with default particle mesh Ewald settings including a direct space cut-off of 9.0 Å (Darden et al., 1993). The temperature was maintained at 300 K using a Langevin thermostat (Loncharich et al., 1992) and a 2 ps⁻¹ collision frequency. Hydrogen mass repartitioning was used to increase masses of hydrogen atoms, allowing a 4 fs timestep (Hopkins et al., 2015). SHAKE was used to constrain bonds to hydrogens (Ryckaert et al., 1977). Trajectory frames were saved every 100 ps.

Umbrella sampling simulations were initiated for each system (Fc(+G + H), Fc(-G + H), Fc(+G-H), and Fc(-G-H)) from two of the four equilibrated structures described above (Kumar et al., 1992, 1995). Each equilibrated structure (2 structures per system) was used as the starting structure of an umbrella sampling window where the center of mass (COM) distance restraint was restrained to every 1.0 Å between 30.0 Å and 55.0 Å (26 windows total). The center of mass distance restraint was defined as the distance between the CH2 domains' centers of mass of the alpha carbon (C-alpha) atoms (Supplementary Figure 3), and each window was restrained with 20.92 kJ/mol Å² (5 kcal/mol Å²) weight restraints. NPT simulations were run for each window for 500 ps. Supplementary Figure 4 shows the COM distance vs. time, indicating each window reached its assigned COM value by the end of the equilibration. After each window was equilibrated at its target COM distance, production umbrella sampling was run for 2 ns at 0.5 Å window intervals from 30.0 Å to 55.0 Å (52 windows total), where the lower 1.0 Å window's equilibrated structure was used as a starting point for the 1.0 Å and 0.5 Å interval umbrella sampling simulations (i.e. the structure equilibrated at 30.0 Å was used as a starting structure for the 30.0 Å and 30.5 Å windows). Supplementary Figure 5 shows the histogram overlap of each 0.5 Å window for the 1.5 ns production dynamics. WHAM was used to generate free energy profiles from the COM distances recorded at every simulation step (2 fs) over the last 1.5 ns of each window (Grossfield, 2020; Kumar et al., 1992).

Starting structures for all systems and the analysis scripts used to generate the data are provided on Github at <https://github.com/cbergonzo/FcHingeGlycans>.

Results

Crystal structure of *E. coli* expressed Fc

The crystal structure of Fc expressed in *E. coli* (PDB ID: 7RHO, Fc(-G-H)) includes four independent copies in the asymmetric unit. The proteins form compact egg-shaped dimers with two Fc molecules interclasped to form a particle 10 nm long

with approximate 222 symmetry (Supplementary Figure 6). A similar arrangement was observed in crystal structure 4D2N of a deglycosylated IgG4 Fc (Davies et al., 2014). The *E. coli* expressed Fc includes heavy chain residues 240-450, and all are visible in at least one of the eight chains, while the two-residue N-terminal extension is likely disordered and is not observed. The four molecules display some variations in loop conformations but superimpose with all pairwise C-alpha root mean squared deviation (RMSD) values under 1.8 Å. The AB molecule is used to represent Fc(-G-H) as the starting structure for MD simulations. Chains A and B overlay onto each other with an RMSD of 0.53 Å and onto the previously reported structure of 5VGP (Fc(+G+H)), with an RMSD of 1.1 Å and 1.2 Å, respectively. Superimposing the entire 7RHO Fc (A and B chains) onto 5VGP raises the C-alpha RMSD to 1.4 Å, largely due to their different separation of CH2 domains, where the domains are 2 Å further apart in 7RHO than in 5VGP.

Molecular dynamics simulations characterize Fc dynamics

MD simulations were conducted on four systems: Fc(-G-H), which has no glycans and no hinge; Fc(-G+H), which has a hinge and no glycans; Fc(+G-H), which has glycans and no hinge; and Fc(+G+H), which has both glycans and hinge (Table 2). Over the course of the microsecond length MD simulations, the Fc(-G-H) and Fc(-G+H) systems, both lacking glycans, were significantly more flexible than Fc(+G-H) and Fc(+G+H), as seen in the average per-residue contributions to the root mean square deviation (RMSD) (Supp. Table 2). Across all four systems the CH2 domain is more mobile than the CH3 domain. The flexible loops at the top of the Fc beta hairpins are responsible for the highest per-residue contribution to the RMSD (fluctuations centered around residues 272, 299, 332 (chains H and V, numbering consistent with NISTmAb intact model and PDB ID: 5VGP) in all systems (Supplementary Figure 7), with the Fc(-G-H) system showing the highest range for overall fluctuation. The trend in average per-residue RMSD reports increased flexibility for systems lacking glycans (Fc(-G+H) and Fc(-G-H)), for both the CH2 and CH3 domains.

Fc domain dynamics can be summarized through conformational analysis relating to specific inter and intra chain angles, dihedrals and distances, reported in Supplementary Table 2 (Frank et al., 2014). Trends indicate slightly more acute angles between the CH2 and CH3 domains in the Fc(-G-H) simulations. The CH2/CH3 dihedral measures the twist of the CH2 and CH3 regions of the Fc domain. Average dihedral values are wider in the Fc(-G-H) system. The CH2/CH2 Asn300 distance measures the distance between N-linked glycan attachment points. The trend shows wider Asn-Asn distances in Fc(-G-H). Overall, while average values tend to be outliers for the Fc(-G-H) system, they are not statistically different from other systems' values, and therefore the dynamics of each Fc system are similar. Additionally, we compare the Fc domain motion in the context of the individual Fc domains to 4 μs of aggregate simulated data for the

intact NISTmAb in Supplementary Figure 8. The internal dynamics shown in the distributions of the CH2-CH3 angle and CH2-CH3 dihedral for the Fc fragment by itself matches the distributions from the Fc domain of the simulated NISTmAb structure. We can conclude that the simulations are sampling similar internal domain dynamics for Fc during these 1 microsecond-length simulations.

Principal component analysis of Fc domain simulations

The principal components were calculated for the common residues of the combined trajectories of each of the four simulated systems (using 5VGP sequence as a reference, residues Ser242 through Leu444 inclusive for each chain) and are shown in Figure 2A (top five modes shown in Supplementary Figure 9). In all systems, the dominant mode of motion corresponds to the CH2 domains of each chain swinging towards and away from each other. The swing directions of the dominant modes for the Fc(-G-H) system deviate from those of the other three and are shown by porcupine plots in Figure 2B. The first PC describes CH2 domains bending directly towards each other in the XY plane, an attribute described by the intra-chain CH2-CH3 angle in Supplementary Table 2. The second PC describes CH2 domains opening and closing in the YZ plane (bending out of the screen). The third through fifth PC projections are more Gaussian in shape (Supplementary Figure 9), indicating the higher frequency motions are more similar and/or better converged. Weights for each PC are reported in Supplementary Table 3.

The PCs of each individual simulation were determined to compare differences between the low-frequency, collective motions sampled by each system. The PCs of the Fc(-G-H) system were distinct from the other three systems, having had the lowest similarity of the first fifteen low frequency modes to any other system as compared using the RMS inner product (RMSIP) (Table 3) (Amadei et al., 1993). The main difference in motion along the first principal component of each system is illustrated in Figure 2B. The absence of both the hinge and glycans in the Fc(-G-H) system enables more direct motion of each chain's CH2 domains directly towards each other (Figure 2B, top). Addition of the glycans both restricts and reorients the PC motions. Addition of the hinge has a similar result.

CH2-CH2 domain opening reports on deformability of the Fc domain

For each system, the first PC described the separation between the CH2 domains of each chain (Figure 2B). Thus, the CH2-CH2 center of mass (COM) distance was used as a reaction coordinate in umbrella sampling simulations (Supplementary Figure 3) to interrogate Fc flexibility outside the well-defined range of local energy minimum described by the equilibrium MD simulations above. The Fc dimer was pushed together to a COM distance of 30.0 Å and pulled apart to a COM distance of 55.0 Å, illustrated in Figure 3A,

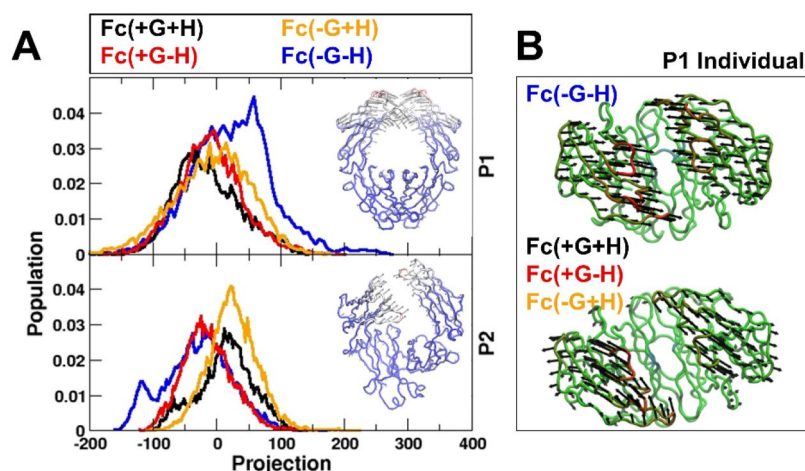


Figure 2. (A) Projection of combined principal components along first two eigenvectors for each Fc truncation system. Images of the Fc domain show porcupine plots describing PC motions. (B) Individually calculated first PC for Fc(-G-H) (top) and Fc(+G+H), Fc(+G-H), Fc(-G+H) (bottom) systems. Red colors indicate residues which have the highest fluctuation along this PC. Porcupine images were made using the Normal Mode Wizard (NMWiz) plugin for Visual Molecular Dynamics (VMD) (Bakan et al., 2011).

Table 3. Rms inner product between all eigenvectors (15) calculated from independent PCA of each system's simulated trajectories.

System	Fc(-G-H)	Fc(+G+H)	Fc(+G-H)	Fc(-G+H)
Fc(-G-H)	1.000	0.839	0.842	0.851
Fc(+G+H)	–	1.000	0.893	0.889
Fc(+G-H)	–	–	1.000	0.899
Fc(-G+H)	–	–	–	1.000

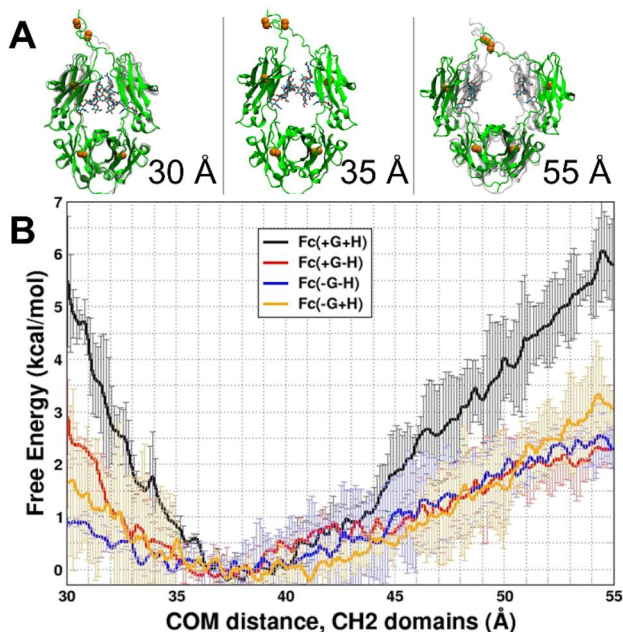


Figure 3. (A) Image of Fc domains at a COM distance of 30 Å, 35 Å and 55 Å. (B) Resulting free energies from umbrella sampling simulations for each system (Fc(+G+H), black; Fc(+G-H), red; Fc(-G+H), yellow; Fc(-G-H), blue). Averages and standard deviations, shown as error bars, are from the last 1.5 ns of two independent 2 ns simulations.

well past the COM ranges observed in crystal structures of Fc (Supplementary Table 1 and Supplementary Figure 1).

Figure 3B shows the resulting free energy profiles from umbrella sampling simulations. With the hinge present (Fc(+G+H) and Fc(-G+H) systems), a covalent link between the two chains exists close to the CH2 domains. Thus, when

the COM distance is increased, the free energy along the reaction coordinate increases due to the strain imposed by deforming the hinge. When the hinge is deleted in the Fc(-G-H) and Fc(+G-H) systems, this covalent linkage bond does not exist and the domains are more easily pulled apart (Figure 3B, black line and yellow line, respectively). Though the trend is present for systems with and without glycans, there is an additional 12.55 kJ/mol (3 kcal/mol) penalty for the Fc(+G+H) system with glycans present, showing that the glycans contribute significant free energy to the stability across the Fc dimer.

When the Fc CH2 COM distance is pushed together, the free energy along the reaction coordinate increases in the Fc(+G+H) and Fc(+G-H) systems where glycans are present (Figure 3B, black line and red line, respectively). In the Fc(-G-H) and Fc(-G+H) systems without glycans (Figure 3B, blue line and yellow line, respectively) there are lower free energies reported since there is no steric clash between CH2 domains. The presence of the hinge in the Fc(+G+H) system adds an additional energy penalty to pushing CH2 domains closer together (+8.37 kJ/mol, +2 kcal/mol).

The free energy curve also displays a broad minimum denoting CH2-CH2 distances from 33 Å to 42 Å occupied at < 4.18 kJ/mol (1 kcal/mol) free energy. The starting distance in the 5VGP crystal structure is 35.7 Å (Supplementary Table 1). This indicates a very flexible Fc domain exists, both in the presence and absence of the hinge and glycans, since it easily adopts structures across the 9 Å wide distance range.

Discussion

Altering CH2 dynamics is a target in engineering therapeutic antibodies (Remesh et al., 2018). A useful prediction algorithm for biopharmaceutical companies would report the stability of a particular Fc domain modification in a reasonably short amount of time (min or h vs. days). To this end, we have sought to develop a computational method that makes use of all-atom molecular dynamics simulations, which have

the necessary per-residue resolution required to understand subtle modifications to Fc that modulate function (Lobner et al., 2016; Ying et al., 2014).

Dihedral and angle measurements between the CH2 and CH3 domains averaged across all long MD simulations agree with measurements of deposited Fc crystal structures, and with the simulations of the intact NISTmAb. Across all four systems the CH2 domain is more mobile than the CH3 domain, in agreement with previous data (Frank et al., 2014). Analysis of the glycans in the microsecond length simulations confirms the observations of flexibility in both branches of each chain's biantennary glycan, measured experimentally by NMR chemical shift (Barb & Prestegard, 2011) and previous molecular dynamics simulations (Fogarty et al., 2020; Turupcu & Oostenbrink, 2017), and shown in the Supplementary Information phi/psi plots of the Man- α (1-3)-Man and Man- α (1-6)-Man linkages (Supplementary Figures 10 and 11). This helps confirm the importance in describing the ensemble dynamics that oscillate around an average Fc structure.

While the average values for all systems were within one standard deviation of each other (Supplementary Table 2), the trend in dynamics of Fc(-G-H) displayed slight differences (Figure 2). The first and second combined principal component projections of the Fc(-G-H) system were non-Gaussian outliers (Figure 2A). Further analysis of the independent systems' principal components (Figure 2B) showed that the Fc(-G-H) system was the most different from the other systems, through the RMSIP of the calculated set of 15 eigenvectors (Table 2). The motion along the first principal component, calculated independently for Fc(-G-H), showed CH2 domains moving directly towards each other. This motion arises due to the lack of covalent linkage between the two protein chains (hinge deleted) and lack of non-covalent interactions between the two CH2 domains (no glycans). The independently calculated first principal components of the other systems (Fc(+G+H), Fc(+G-H), Fc(-G+H)) show CH2 domains moving at an angle, avoiding collision of either hinge, glycans, or both. Note that a simple RMSF measurement in this case would be of little help to define differences in these dynamics (Supplementary Figure 7), as the same CH2 domain residues fluctuate in each mode – the direction-dependent motion is important to consider here, and points to the difficulty of creating robust measurements of biomolecular dynamics for these systems.

Fc domain opening is a well-studied phenomenon since Fc receptors bind at this location. To quantify the Fc dynamics beyond the local energy minimum sampled in the long timescale all-atom molecular dynamics simulations, we ran umbrella sampling simulations to explore more conformational space. We used umbrella sampling along a reaction coordinate that pulled apart and pushed together each chain's CH2 domains, to probe past distances observed in either simulation or crystal structures of Fc (Supplementary Figure 1, Supplementary Table 1). By distributing the biasing energy for the conformational change along all CH2 domain alpha carbon atoms (104 atoms per domain in total, Supplementary Figure 3), we were able to decompose free

energies along this reaction coordinate, from an over-closed distance of 35 Å to a wide distance of 55 Å. These values were outside those measured in crystal structures of Fc domains (Supplementary Figure 1, Supplementary Table 1).

The presence or absence of glycans has the largest effect on the free energy when the distance between CH2 domains is short. When glycans are absent (Fc(-G-H) and Fc(-G+H) systems), the domains are more easily pushed together. However, the presence of the hinge in the Fc(-G+H) system introduces a source of steric penalty between the domains, slightly raising the free energy at low distances. When glycans are present, a larger free energy penalty is present. The results are consistent with measured RMSD values which indicate that the presence of glycans stabilize the dimer across its interface, and result in lower fluctuations overall, including in the CH3 domains (Supplementary Table 2).

The presence or absence of the hinge has the largest effect on free energy when CH2 domains are pulled apart. When the hinge is present, the covalent linkage provided by the two disulfide bonds prevents the domains from being pulled apart easily, that is, there is a higher free energy penalty at longer COM distances. When the hinge is absent, it is much easier to pull the CH2 domains apart. Though the above trend is present in the hinge (+/-) systems, there is a significant decrease in free energy while pulling CH2 domains apart when glycans are absent in the Fc(-G+H) system compared to glycans present in the Fc(+G+H) system. This proves that glycans contribute a significant amount of energy to stabilizing the Fc domain dimer. To further examine the role of the glycans, we looked at their interactions as a function of Fc opening. We observed glycan interactions persist longer when the hinge is absent, most likely due to the unrestricted motion in the CH2 domains (Supplementary Figure 12).

Conclusion

The Fc domain might be thought of as the less flexible domain of an IgG, but its dynamics play an important role in both determining and engineering function. Though averages from molecular dynamics simulations faithfully reproduce values observed in crystal structures, the dynamic motions of the various Fc hinge and glycan truncations, examined using principal component analysis, report on key differences. We have shown that upon pulling the Fc dimer apart to 55 Å, the presence of the hinge and glycans results in a 16.74 kJ/mol (4 kcal/mol) free energy increase over systems with no hinge present, and that the presence of glycans contributes 12.55 kJ/mol (3 kcal/mol) free energy to Fc domain stabilization. Upon dimer constriction to 30 Å, the presence of the glycans results in a 12.55 kJ/mol to 20.92 kJ/mol (3 kcal/mol to 5 kcal/mol) free energy increase over systems without glycans present, with the presence of the hinge contributing 8.37 kJ/mol free energy over the hingeless system (2 kcal/mol). The umbrella sampling simulations presented here probe Fc domain destabilization with high precision, and report stability values in terms of free energy on several Fc domain modifications.

Acknowledgments

C.B. would like to acknowledge computational resources from UMD and NIST administered at IBRR.

Author disclaimer

Certain equipment, instruments, software, or materials, commercial or non-commercial, are identified in this paper in order to specify the experimental procedure adequately. Such identification is not intended to imply recommendation or endorsement of any product or service by NIST, nor is it intended to imply that the materials or equipment identified are necessarily the best available for the purpose.

Disclosure statement

The authors declare no conflict of interest.

Funding

GM/CA@APS has been funded by the National Cancer Institute (ACB-12002) and the National Institute of General Medical Sciences (AGM-12006, P30GM138396). This research used resources of the Advanced Photon Source, a U.S. Department of Energy (DOE) Office of Science User Facility operated for the DOE Office of Science by Argonne National Laboratory under Contract No. DE-AC02-06CH11357. This work was supported by the NIST Biomanufacturing grant.

References

- Amadei, A., Linssen, A. B. M., & Berendsen, H. J. C. (1993). Essential dynamics of proteins. *Proteins*, 17(4), 412–425. <https://doi.org/10.1002/prot.340170408>
- Anandakrishnan, R., Baker, C., Izadi, S., & Onufriev, A. V. (2013). Point charges optimally placed to represent the multipole expansion of charge distributions. *PLoS One*, 8(7), e67715. <https://doi.org/10.1371/journal.pone.0067715>
- Bakan, A., Meireles, L. M., & Bahar, I. (2011). ProDy: Protein dynamics inferred from theory and experiments. *Bioinformatics*, 27(11), 1575–1577. <https://doi.org/10.1093/bioinformatics/btr168>
- Barb, A. W., & Prestegard, J. H. (2011). NMR analysis demonstrates immunoglobulin G N-glycans are accessible and dynamic. *Nature Chemical Biology*, 7(3), 147–153. <https://doi.org/10.1038/nchembio.511>
- Berendsen, H. J. C., Grigera, J. R., & Straatsma, T. P. (1987). The missing term in effective pair potentials. *Journal of Physical Chemistry*, 91(24), 6269–6271. <https://doi.org/10.1021/j100308a038>
- Bergonzo, C., & Gallagher, D. T. (2021). Atomic Model Structure of the NIST Monoclonal Antibody (NISTmAb) Reference Material (RM). *Journal of Research of the National Institute of Standards*, 126(126012), 1–6. <https://doi.org/10.6028/jres.126.012>
- Buck, P. M., Kumar, S., & Singh, S. K. (2013). Consequences of glycan truncation on Fc structural integrity. *MAbs*, 5(6), 904–916. <https://doi.org/10.4161/mabs.26453>
- Chiu, M. L., Goulet, D. R., Teplyakov, A., & Gilliland, G. L. (2019). Antibody structure and function: The basis for engineering therapeutics. *Antibodies*, 8(4), 55. <https://doi.org/10.3390/antib8040055>
- Dall'Acqua, W. F., Cook, K. E., Damschroder, M. M., Woods, R. M., & Wu, H. (2006). Modulation of the effector functions of a human IgG1 through engineering of its hinge region. *The Journal of Immunology*, 177(2), 1129–1138. <https://doi.org/10.4049/jimmunol.177.2.1129>
- Darden, T., York, D., & Pedersen, L. (1993). Particle mesh Ewald: An Nlog(N) method for Ewald sums in large systems. *Journal of Chemical Physics*, 98, 10089–10092. <https://doi.org/10.1063/1.464397>
- Davies, A. M., Jefferis, R., & Sutton, B. J. (2014). Crystal structure of deglycosylated human IgG4-Fc. *Molecular Immunology*, 62(1), 46–53. <https://doi.org/10.1016/J.MOLIMM.2014.05.015>
- Deveuve, Q., Lajoie, L., Barrault, B., & Thibault, G. (2020). The proteolytic cleavage of therapeutic monoclonal antibody hinge region: More than a matter of subclass. *Frontiers in Immunology*, 11, 168. <https://doi.org/10.3389/fimmu.2020.00168>
- Duivelshof, B. L., Murisier, A., Camperi, J., Fekete, S., Beck, A., Guillaume, D., & D'Atri, V. (2021). Therapeutic Fc-fusion proteins: Current analytical strategies. *Journal of Separation Science*, 44(1), 35–62. <https://doi.org/10.1002/jssc.202000765>
- Fogarty, C. A., Harbison, A. M., Dugdale, A. R., & Fadda, E. (2020). How and why plants and human N-glycans are different: Insight from molecular dynamics into the “glycoblocks” architecture of complex carbohydrates. *Beilstein Journal of Organic Chemistry*, 16, 2046–2056. <https://doi.org/10.3762/BJOC.16.171>
- Frank, M., Walker, R. C., Lanzilotta, W. N., Prestegard, J. H., & Barb, A. W. (2014). Immunoglobulin G1 Fc domain motions: Implications for Fc engineering. *Journal of Molecular Biology*, 426(8), 1799–1811. <https://doi.org/10.1016/j.jmb.2014.01.011>
- Gallagher, D. T., Galvin, C. V., & Karageorgos, I. (2018). Structure of the Fc fragment of the NIST reference antibody RM8671. *Acta Crystallographica Section F*, 74(9), 524–529. <https://doi.org/10.1107/S2053230X18009834>
- Grossfield, A. (2020) WHAM: the weighted histogram analysis method (Version 2.0.10). <http://membrane.urmc.rochester.edu/content/wham>
- Harbison, A., & Fadda, E. (2020). An atomistic perspective on antibody-dependent cellular cytotoxicity quenching by core-fucosylation of IgG1 Fc N-glycans from enhanced sampling molecular dynamics. *Glycobiology*, 30(6), 407–414. <https://doi.org/10.1093/glycob/cwz101>
- Harris, L. J., Larson, S. B., Hasel, K. W., & McPherson, A. (1997). Refined structure of an intact IgG2a monoclonal antibody. *Biochemistry*, 36(7), 1581–1597. <https://doi.org/10.1021/bi962514+>
- Hopkins, C. W., Le Grand, S., Walker, R. C., & Roitberg, A. E. (2015). Long time step molecular dynamics through hydrogen mass repartitioning. *Journal of Chemical Theory and Computation*, 11(4), 1864–1874. <https://doi.org/10.1021/ct5010406>
- Humphrey, W., Dalke, A., & Schulten, K. (1996). VMD: visual molecular dynamics. *Journal of Molecular Graphics*, 14(1), 33–38. [https://doi.org/10.1016/0263-7855\(96\)00018-5](https://doi.org/10.1016/0263-7855(96)00018-5)
- Jafari, R., Zolbanin, N. M., Rafatpanah, H., Majidi, J., & Kazemi, T. (2017). Fc-fusion Proteins in Therapy: An Updated View. *Current Medicinal Chemistry*, 24(12), 1228–1237. <https://doi.org/10.2174/0929867324666170113112759>
- Joung, I. S., & Cheatham, T. E. (2008). Determination of alkali and halide monovalent ion parameters for use in explicitly solvated biomolecular simulations. *Journal of Physical Chemistry B*, 112(30), 9020–9041. <https://doi.org/10.1021/jp8001614>
- Karageorgos, I., Gallagher, E. S., Galvin, C., Gallagher, D. T., & Hudgens, J. W. (2017). Biophysical characterization and structure of the Fab fragment from the NIST reference antibody, RM 8671. *Biologicals*, 50, 27–34. <https://doi.org/10.1016/j.biologics.2017.09.005>
- Kirschner, K. N., Yongye, A. B., Tschampel, S. M., González-Outeiriño, J., Daniels, C. R., Foley, B. L., & Woods, R. J. (2008). GLYCAM06: A generalizable biomolecular force field. *Carbohydrates. Journal of Computational Chemistry*, 29(4), 622–655. <https://doi.org/10.1002/jcc.20820>
- Kiyoshi, M., Caaveiro, J. M. M., Kawai, T., Tashiro, S., Ide, T., Asaoka, Y., Hatayama, K., & Tsumoto, K. (2015). Structural basis for binding of human IgG1 to its high-affinity human receptor FcγRI. *Nature Communications*, 6(1), 1–11. <https://doi.org/10.1038/ncomms7866>
- Kiyoshi, M., Tsumoto, K., Ishii-Watabe, A., & Caaveiro, J. M. M. (2017). Glycosylation of IgG-Fc: a molecular perspective. *International Immunology*, 29(7), 311–317. <https://doi.org/10.1093/INTIMM/DXX038>
- Krissinel, E., & Henrick, K. (2007). Inference of macromolecular assemblies from crystalline state. *Journal of Molecular Biology*, 372(3), 774–797. <https://doi.org/10.1016/j.jmb.2007.05.022>
- Kumar, S., Rosenberg, J. M., Bouzida, D., Swendsen, R. H., & Kollman, P. A. (1992). THE weighted histogram analysis method for free-energy calculations on biomolecules. I. The method. *Journal of Computational Chemistry*, 13(8), 1011–1021. <https://doi.org/10.1002/jcc.540130812>
- Kumar, S., Rosenberg, J. M., Bouzida, D., Swendsen, R. H., & Kollman, P. A. (1995). Multidimensional free-energy calculations using the

- weighted histogram analysis method. *Journal of Computational Chemistry*, 16(11), 1339–1350. <https://doi.org/10.1002/jcc.540161104>
- Lai, B., Hasenhiindl, C., Obinger, C., & Oostenbrink, C. (2014). Molecular dynamics simulation of the crystallizable fragment of IgG1—Insights for the design of fcabs. *International Journal of Molecular Sciences*, 15(1), 438–455. <https://doi.org/10.3390/ijms15010438>
- Lee, H. S., & Im, W. (2017). Effects of N-Glycan Composition on Structure and Dynamics of IgG1 Fc and Their Implications for Antibody Engineering. *Scientific Reports*, 7(1), 12659. <https://doi.org/10.1038/s41598-017-12830-5>
- Lobner, E., Traxlmayr, M. W., Obinger, C., & Hasenhiindl, C. (2016). Engineered IgG1-Fc - one fragment to bind them all. *Immunological Reviews*, 270(1), 113–131. <https://doi.org/10.1111/imr.12385>
- Loncharich, R. J., Brooks, B. R., & Pastor, R. W. (1992). Langevin dynamics of peptides: the frictional dependence of isomerization rates of N-acetylalanyl-N'-methylamide. *Biopolymers*, 32(5), 523–535. <https://doi.org/10.1002/bip.360320508>
- Losonczi, J. A., & Prestegard, J. H. (1998). Improved dilute bicelle solutions for high-resolution NMR of biological macromolecules. *Journal of Biomolecular NMR*, 12(3), 447–451. <https://doi.org/10.1023/A:1008302110884>
- Ma, B. (2021). Correlation of N-glycan dynamics and interaction network with allosteric antigen binding and Fc receptor recognition. *Exploration of Immunology*, 1(1), 27–36. <https://doi.org/10.37349/ei.2021.00004>
- Maier, J. A., Martinez, C., Kasavajhala, K., Wickstrom, L., Hauser, K. E., & Simmerling, C. (2015). ff14SB: Improving the Accuracy of Protein Side Chain and Backbone Parameters from ff99SB. *Journal of Chemical Theory and Computation*, 11(8), 3696–3713. <https://doi.org/10.1021/acs.jctc.5b00255>
- McCoy, A. J., Grosse-Kunstleve, R. W., Adams, P. D., Winn, M. D., Storoni, L. C., & Read, R. J. (2007). Phaser crystallographic software. *Journal of Applied Crystallography*, 40(4), 658–674. <https://doi.org/10.1107/S0021889807021206>
- Murshudov, G. N., Vagin, A. A., & Dodson, E. J. (1997). Refinement of macromolecular structures by the maximum-likelihood method. *Acta Crystallographica Section D: Biological Crystallography*, 53(3), 240–255. <https://doi.org/10.1107/S0907444996012255>
- Presta, L. G. (2008). Molecular engineering and design of therapeutic antibodies. *Current Opinion in Immunology*, 20(4), 460–470. <https://doi.org/10.1016/j.coi.2008.06.012>
- Prien, J. M., Stöckmann, H., Albrecht, S., Martin, S. M., Varatta, M., Furtado, M., Hosselet, S., Wang, M., Formolo, T., Rudd, P. M., & Schiel, J. E. (2015). Orthogonal technologies for NISTmAb N-glycan structure elucidation and quantitation. *ACS Symposium Series*, 1201(i), 185–235. <https://doi.org/10.1021/bk-2015-1201.ch004>
- Remesh, S. G., Armstrong, A. A., Mahan, A. D., Luo, J., & Hammel, M. (2018). Conformational Plasticity of the Immunoglobulin Fc Domain in Solution. *Structure*, 26(7), 1007–1014.e2. <https://doi.org/10.1016/j.str.2018.03.017>
- Roe, D. R., & Bergonzo, C. (2022). prepareforleap: An automated tool for fast PDB-to-parameter generation. *Journal of Computational Chemistry*, 43(13), 930–935. <https://doi.org/10.1002/jcc.26847>
- Roe, D. R., & Brooks, B. R. (2020). A protocol for preparing explicitly solvated systems for stable molecular dynamics simulations. *Journal of Chemical Physics*, 153(5), 054123. <https://doi.org/10.1063/5.0013849>
- Russell, A., Adua, E., Ugrina, I., Laws, S., & Wang, W. (2018). Unravelling immunoglobulin G Fc N-glycosylation: A dynamic marker potentiating predictive, preventive and personalised medicine. *International Journal of Molecular Sciences*, 19(390), 1–18. <https://doi.org/10.3390/ijms19020390>
- Ryckaert, J.-P., Ciccotti, G., & Berendsen, H. J. C. (1977). Numerical integration of the cartesian equations of motion of a system with constraints: molecular dynamics of n-alkanes. *J. Comput. Phys.*, 23(3), 327–341. [https://doi.org/10.1016/0021-9991\(77\)90098-5](https://doi.org/10.1016/0021-9991(77)90098-5)
- Salomon-Ferrer, R., Götz, A. W., Poole, D., Le Grand, S., & Walker, R. C. (2013). Routine microsecond molecular dynamics simulations with AMBER on GPUs. 2. Explicit solvent particle mesh Ewald. *Journal of Chemical Theory and Computation*, 9(9), 3878–3888. <https://doi.org/10.1021/ct400314y>
- Schiel, J.E., Mire-Sluis, A., & Davis, D. (2014). State-of-the-art and emerging Technologies for Therapeutic Monoclonal Antibody Characterization Volume 1. Monoclonal antibody therapeutics: structure, function, and regulatory space. ACS Symposium Series, 1–34.
- Schiel, J.E., Turner, A., Mouchahoir, T., Yandrofski, K., Telikepalli, S., King, J., DeRose, P., Ripple, D., & Phinney, K. (2018). The NISTmAb Reference Material 8671 value assignment, homogeneity, and stability. *Analytical and Bioanalytical Chemistry*, 410(8), 2127–2139. <https://doi.org/10.1007/S00216-017-0800-1/FIGURES/10>
- Schrödinger, L., & DeLano, W. (2020). *PyMOL*.
- Sengupta, A., Li, Z., Song, L. F., Li, P., & Merz, K. M. (2021). Parameterization of monovalent ions for the OPC3, OPC, TIP3P-FB, and TIP4P-FB water models. *Journal of Chemical Information and Modeling*, 61(2), 869–880. <https://doi.org/10.1021/acs.jcim.0c01390>
- Tian, C., Kasavajhala, K., Belfon, K. A. A., Raguette, L., Huang, H., Miguez, A. N., Bickel, J., Wang, Y., Pincay, J., Wu, Q., & Simmerling, C. (2020). Ff19SB: Amino-acid-specific protein backbone parameters trained against quantum mechanics energy surfaces in solution. *Journal of Chemical Theory and Computation*, 16(1), 528–552. <https://doi.org/10.1021/acs.jctc.9b00591>
- Traxlmayr, M. W., Wozniak-Knopp, G., Antes, B., Stadlmayr, G., Rüker, F., & Obinger, C. (2011). Integrin binding human antibody constant domains-Probing the C-terminal structural loops for grafting the RGD motif. *Journal of Biotechnology*, 155(2), 193–202. <https://doi.org/10.1016/j.jbiotec.2011.06.042>
- Turupcu, A., & Oostenbrink, C. (2017). Modeling of oligosaccharides within glycoproteins from free-energy landscapes. *Journal of Chemical Information and Modeling*, 57(9), 2222–2236. <https://doi.org/10.1021/acs.jcim.7b00351>
- Valeich, J., Boyd, D., Kanwar, M., Stenzel, D., De Ghosh, D., Ebrahimi, A., Woo, J., Wang, J., & Ambrogelly, A. (2020). Taking the hinge off: an approach to effector-less monoclonal antibodies. *Antibodies*, 9(50), 1–14. <https://doi.org/10.3390/antib9040050>
- Winn, M. D., Ballard, C. C., Cowtan, K. D., Dodson, E. J., Emsley, P., Evans, P. R., Keegan, R. M., Krissinel, E. B., Leslie, A. G. W., McCoy, A., McNicholas, S. J., Murshudov, G. N., Pannu, N. S., Potterton, E. A., Powell, H. R., Read, R. J., Vagin, A., & Wilson, K. S. (2011). Overview of the CCP4 suite and current developments. *Acta Crystallographica Section D*, 67(4), 235–242. <https://doi.org/10.1107/S0907444910045749>
- Wozniak-Knopp, G., Bartl, S., Bauer, A., Mostageer, M., Woisetschläger, M., Antes, B., Ettl, K., Kainer, M., Weberhofer, G., Wiederkum, S., Himmler, G., Mudde, G. C., & Rüker, F. (2010). Introducing antigen-binding sites in structural loops of immunoglobulin constant domains: Fc fragments with engineered HER2/neu-binding sites and antibody properties. *Protein Engineering, Design and Selection*, 23(4), 289–297. <https://doi.org/10.1093/protein/gzq005>
- Yan, B., Boyd, D., Kaschak, T., Tsukuda, J., Shen, A., Lin, Y., Chung, S., Gupta, P., Kamath, A., Wong, A., Vernes, J. M., Meng, G. Y., Totpal, K., Schaefer, G., Jiang, G., Nogal, B., Emery, C., Vanderlaan, M., Carter, P., ... Amanullah, A. (2012). Engineering upper hinge improves stability and effector function of a human IgG1. *Journal of Biological Chemistry*, 287(8), 5891–5897. <https://doi.org/10.1074/jbc.M111.311811>
- Yanaka, S., Yogo, R., Inoue, R., Sugiyama, M., Itoh, S. G., Okumura, H., Miyanoiri, Y., Yagi, H., Satoh, T., Yamaguchi, T., & Kato, K. (2019). Dynamic views of the fc region of immunoglobulin G provided by experimental and computational observations. *Antibodies*, 8(3), 39–52. <https://doi.org/10.3390/antib8030039>
- Ying, T., Gong, R., Ju, T. W., Prabakaran, P., & Dimitrov, D. S. (2014). Engineered Fc based antibody domains and fragments as novel scaffolds. *Biochimica et Biophysica Acta - Proteins and Proteomics*, 1844(11), 1977–1982. <https://doi.org/10.1016/j.bbapap.2014.04.018>